Available online at www.sciencedirect.com
SCIENCE DIRECT®
Journal of Computational Physics 195 (2004) 320–340
JOURNAL OF COMPUTATIONAL PHYSICS
www.elsevier.com/locate/jcp

# Numerical problems in semiconductor simulation using the hydrodynamic model: a second-order finite difference scheme ☆

Luca V. Ballestra [a], Riccardo Sacco [b,*]

[a] *Dipartimento di Matematica, Università di Milano, "F. Enriques", Via Saldini 50, 20133 Milan, Italy*
[b] *Dipartimento di Matematica, MOX, Modeling and Scientific Computing, "F. Brioschi", Politecnico di Milano, Via Bonardi 9, 20133 Milan, Italy*

Received 10 May 2001; received in revised form 30 July 2003; accepted 6 October 2003

**Abstract**

In this paper, a second-order Total Variation Diminishing (TVD) finite difference scheme of upwind type is employed for the numerical approximation of the classical hydrodynamic model for semiconductors proposed by Bløtekjær and Baccarani–Wordeman. In particular, the high-order hyperbolic fluxes are evaluated by a suitable extrapolation on adjacent cells of the first-order fluxes of Roe, while total variation diminishing is achieved by limiting the slopes of the discrete Riemann invariants using the so-called *Flux Corrected Transport* approach. Extensive numerical simulations are performed on a submicron $n^+ - n - n^+$ ballistic diode. The numerical experiments show that the spurious oscillations arising in the electron current are not completely suppressed by the TVD scheme, and can lead to serious numerical instabilities when the solution of the hydrodynamic model is non-smooth and the computational mesh is coarse. The accuracy of the numerical method is investigated in terms of conservation of the steady electron current. The obtained results show that the second-order scheme does not behave much better than a corresponding first-order one due to a poor performance of the slope limiters caused by the presence of local extrema of the Riemann invariant associated with the hyperbolic system.


## 1. Introduction

In this work, the classical hydrodynamic model (HD) for semiconductors developed by Bløtekjær (see [10]) and Baccarani and Wordeman (see [6]), is numerically approximated by a second-order TVD finite difference scheme.

☆ The first author was partially supported by the Initiative "Giovani Ricercatori", Politecnico di Milano. The second author was supported by the M.U.R.S.T. Grant Cofin 2001, "Advanced Numerical Methods for Partial Differential Equations of Applicative Interest".
* Corresponding author.
*E-mail address:* ricsac@mate.polimi.it (R. Sacco).

0021-9991/$ - see front matter 
doi:10.1016/j.jcp.2003.10.002

High resolution schemes have been largely applied, in the last 30 years, in compressible aerodynamics for the numerical computation of shocks, since they may resolve strong discontinuities without smearing effects or generating spurious oscillations.

In semiconductor device simulation, high-order shock capturing algorithms have been applied in [17,19], where the HD model is solved by a third-order ENO finite difference approximation, and in [3–5], where the second-order Nessyahu–Tadmor finite difference scheme is used for the solution of an improved hydrodynamic model including viscous terms in the momentum-energy equations. In the aforementioned papers, numerical simulations of the one-dimensional $n^+ - n - n^+$ diode are presented to illustrate the performance of the discretization method. The computed solutions show the non-monotonicity of the steady electron current profile, that is affected by spurious oscillations which become very large near the drain junction of the device. This can be a serious problem in real-life applications, since the current is usually the most relevant outcome of numerical simulation. Current flux conservation is thus a property of main concern in semiconductor device modeling, and to the authors' knowledge it appears that a thorough investigation of the influence of the oscillations in the current profile on the numerical convergence of numerical schemes for hydrodynamic models is still lacking.

In the present work, dealing with the same benchmark device as in the references above, we want to investigate whether and how much the convergence of the TVD high-order finite difference scheme used in the HD simulation is affected by the (possible) non-monotonicity of the computed solution.

The numerical method adopted in this paper is a suitable extension to the vector case of the well-known second-order fully upwinded scalar discretization developed by Osher and Chakravarthy in [13]. The high-order fluxes are discretized by a suitable extrapolation on adjacent cells of the first-order fluxes of Roe, and total variation diminishing is achieved by limiting the slopes of the discrete Riemann invariants, according to the so-called *Flux Corrected Transport* approach (FCT), originally developed by Boris and Book (see [11,12]) and applied to the discretization of the HD model for semiconductors in [1,2]. With this aim, several slope limiters are employed in numerical computations, as extensively discussed in Section 4 of the paper.

The evaluation of the high-order fluxes by extrapolation of the first-order fluxes does not require the use of an approximate Riemann solver, so that the numerical stability of the method can be furtherly enhanced by performing a semi-implicit time discretization of the relaxation terms in the hydrodynamic model. Moreover, the choice of a fully upwinded method attempts to minimize the loss of accuracy due to artificial diffusion, since, if compared to a central scheme, an upwinded discretization uses the information of the characteristic directions to introduce a smaller amount of numerical viscosity in the discrete counterpart of the hyperbolic system.

Extensive numerical experiments are performed in the simulation of a semiconductor model device, namely, a $n^+ - n - n^+$ one-dimensional diode, which is a prototype of the channel region of a submicron MOS transistor widely employed in contemporary microelectronics technology.

Computations are carried out at an external temperature of 77 K to investigate the convergence of the discretization method proposed in this paper in the numerical solution of the HD system at supersonic regime conditions. In particular, it is shown that the scheme, despite being TVD, does not entirely remove the spurious oscillations in the computed solution. These oscillations are the main responsible of convergence breakdown when the solution of the hydrodynamic model is non-smooth and the computational mesh is coarse. The simulations show also that the high resolution scheme does not achieve much better accuracy than the low-order one, as far as the evaluation of the electron current at steady state is concerned, due to a poor performance of the slope limiters caused by the presence of local extrema of the Riemann invariant associated with the hyperbolic system.

The work is organized as follows: in Section 2 the hydrodynamic model is briefly described. Then, the numerical method is presented in Section 3, where the FCT technique is applied to systems of conservation laws via Roe linearization. The numerical experiments are discussed in Section 4, while some conclusions are drawn in Section 5.

## 2. The hydrodynamic model

The hydrodynamic model for electron charge transport in semiconductor comprises the following conservation laws for electron mass, momentum and energy

$$\begin{cases} \dfrac{\partial n}{\partial t} + \operatorname{div}(n\mathbf{v}) = 0, \\ \dfrac{\partial (n\mathbf{v})}{\partial t} + \operatorname{div}(n\mathbf{v} \otimes \mathbf{v} + nRT\mathbf{I}) + \dfrac{n\mathbf{v}}{\tau_p} = -\dfrac{q_n}{m} n\mathbf{E}, \\ \dfrac{\partial (ne)}{\partial t} + \operatorname{div}(ne\mathbf{v} + nRT\mathbf{v} + \mathbf{q}) + \dfrac{ne - ne_0}{\tau_w} = -\dfrac{q_n}{m} n\mathbf{E} \cdot \mathbf{v}. \end{cases} \tag{1}$$

In (1), $n$ is the electron density, $\mathbf{v} = (u_1, u_2, u_3)^{\mathrm{T}}$ is the electron velocity and $e$ the total energy per unit mass, defined as $e = 3/2RT + 1/2|\mathbf{v}|^2$, where $T$ is the absolute electron temperature, $R = K_{\mathrm{B}}/m$, $m$ is the electron effective mass, $K_{\mathrm{B}}$ is the Boltzmann constant, $|\mathbf{v}|$ is the magnitude of the velocity vector, $(\mathbf{v} \otimes \mathbf{v})_{ij} = u_i u_j$, and $\mathbf{I}$ is the identity matrix. Moreover, $\mathbf{q}$ is the heat flux, $\tau_p$ and $\tau_w$ are the characteristic times for the relaxation of momentum and energy, respectively, and $e_0 = 3/2RT_0$ is the internal energy of the lattice, $T_0$ being the temperature corresponding to thermodynamic equilibrium. Finally, $q_n$ is the electron charge ($> 0$) and $\mathbf{E}$ is the electric field.

The hydrodynamic system (1) must be coupled with the Poisson equation for the electric field

$$\operatorname{div}(\epsilon \mathbf{E}) = q_n(N - n) \tag{2}$$

supported by the constitutive relation

$$\mathbf{E} = -\nabla \phi \tag{3}$$

between the electric field and the electrostatic potential $\phi$. In (2), $\epsilon$ is the dielectric permittivity of the semiconductor medium and $N$ is a given function that models the doping profile in the semiconductor device.

Notice that the hyperbolic part of the hydrodynamic system (1) corresponds exactly to the Euler equations for compressible fluids. Nevertheless, if compared to a gas dynamics problem, the hydrodynamic model for semiconductors is more challenging to deal with, due to the high electric fields that are experienced in submicron devices where strong variations of the doping profile occur (see Section 3). As for the constitutive relations in (1), the heat flux is described by the Fourier-type relation

$$\mathbf{q} = -k\nabla T, \tag{4}$$

where the heat conductivity $k$ is given by the Wiedemann–Franz law

$$k = k_{\mathrm{W-F}} \frac{\mu_0}{m q_n} K_{\mathrm{B}}^2 n T_0 \tag{5}$$

and the relaxation times are given by the Baccarani–Wordeman relations

$$\tau_p = m \frac{\mu_0}{q_n} \frac{T_0}{T}, \quad \tau_w = m \frac{\mu_0}{2q_n} \frac{T_0}{T} + \frac{3}{2} \frac{\mu_0}{q_n v_s^2} K_{\mathrm{B}} T_0,$$

where the low-field mobility $\mu_0$ obeys the following law:

$$\mu_0 = \frac{\Delta \mu}{1 + (N/N_{\mathrm{ref}})^{\alpha}}$$

$\Delta\mu$, $N_{\mathrm{ref}}$ and $\alpha$ being suitable parameters depending on $T_0$.

The parameter $k_{W-F}$ appearing in (5), which measures the amount of heat dissipation, is left unspecified in order to perform a parametric study about its influence on the numerical solution (see Section 4).

## 3. The numerical method

The numerical method used to approximate the hydrodynamic system of conservation laws (1) is a Total Variation Diminishing (TVD) second-order fully one-side upwinded finite difference scheme.

Rigorously speaking, TVD is a purely scalar property, which ensures that spurious oscillations are completely removed from the numerical solution of a nonlinear conservation law, as shown by Harten in [18]. A rigorous extension of this concept to the vector case can only be done for linear hyperbolic systems with constant coefficients, that, passing to the characteristic variables, are equivalent to a diagonal system of scalar hyperbolic equations. Hence, we have decided to use for the numerical approximation of the hydrodynamic problem, a finite difference scheme that is TVD when applied to nonlinear scalar conservation laws and to linear hyperbolic systems with constant coefficients.

### 3.1. TVD fully upwinded semi-discretization of a linear hyperbolic equation

For ease of presentation, we describe the numerical method and its properties starting from the discretization of the model linear hyperbolic equation

$$\frac{\partial u}{\partial t}+\frac{\partial f(u)}{\partial x}=0 \tag{6}$$

on the space–time domain $x \in \mathbb{R}$, $t > 0$, where $f(u) = au$, $a$ being a real constant.

With this aim, let us introduce a uniform time–space grid of collocation nodes $t_k$ and $x_i$, and define time and space intervals $\Delta t = t_{k+1} - t_k$ and $\Delta X = x_{i+1} - x_i$. Then, let us consider the spatial discretization of the flux derivative

$$\left.\frac{\partial f}{\partial x}\right|_{x_i} \doteq \frac{1}{\Delta X}\left(f^{\text{high}}_{i+1/2}-f^{\text{high}}_{i-1/2}\right), \tag{7}$$

where

$$f^{\text{high}}_{i+1/2}=a^{+}u_i+a^{-}u_{i+1}+\frac{1}{2}a^{+}(u_i-u_{i-1})-\frac{1}{2}a^{-}(u_{i+2}-u_{i+1}) \tag{8}$$

and

$$a^{\pm}=\frac{1}{2}(a\pm|a|). \tag{9}$$

The discretization (7)–(9) is a second-order fully upwinded 5-point scheme, where the high-order flux (8) is evaluated starting from the low-order flux

$$f^{\text{low}}_{i+1/2}=\frac{1}{2}(f_{i+1}+f_i)-\frac{1}{2}|a|(u_{i+1}-u_i) \tag{10}$$

and performing the following fully one-side upwinded extrapolation on adjacent cells (see [14,20])

$$f^{\text{high}}_{i+1/2}=f^{\text{low}}_{i+1/2}+\frac{1}{2}\left(f_i-f^{\text{low}}_{i-1/2}\right)+\frac{1}{2}\left(f_{i+1}-f^{\text{low}}_{i+3/2}\right), \tag{11}$$

where $f_k = au_k$ at each space grid point $x_k$. Substituting (8) in (7) one gets

$$\left.\frac{\partial f}{\partial x}\right|_{x_i} \equiv \left.\frac{\delta f}{\delta x}\right|_{x_i} \doteq \frac{a^+}{\Delta X}(u_i - u_{i-1}) + \frac{a^-}{\Delta X}(u_{i+1} - u_i) + \frac{a^+}{\Delta X}\frac{(u_i - u_{i-1})}{2} - \frac{a^+}{\Delta X}\frac{(u_{i-1} - u_{i-2})}{2} + \frac{a^-}{\Delta X}\frac{(u_{i+1} - u_i)}{2} - \frac{a^-}{\Delta X}\frac{(u_{i+2} - u_{i+1})}{2}. \tag{12}$$

Let us now discretize the time derivative in (6) by the forward Euler scheme, so that the numerical approximation of (6) becomes

$$\frac{u_i^{k+1} - u_i^k}{\Delta t} + \left.\frac{\delta f}{\delta x}\right|_{x_i}^k = 0 \tag{13}$$

$\left.\frac{\delta f}{\delta x}\right|_{x_i}^k$ being given by (12) where each quantity $u_j$ is evaluated at the time level $t_k$.

The approximation (12) and (13) is *not* TVD, and, in order to achieve total variation diminishing, we apply the so-called *Flux Corrected Transport* technique (FCT). Following this approach, relation (12) is replaced with

$$\left.\frac{\delta f}{\delta x}\right|_{x_i} = \frac{a^+}{\Delta X}(u_i - u_{i-1}) + \frac{a^-}{\Delta X}(u_{i+1} - u_i) + \frac{a^+}{\Delta X}\Psi^+_{i-1/2}\frac{(u_i - u_{i-1})}{2} - \frac{a^+}{\Delta X}\Psi^+_{i-3/2}\frac{(u_{i-1} - u_{i-2})}{2} + \frac{a^-}{\Delta X}\Psi^-_{i+1/2}\frac{(u_{i+1} - u_i)}{2} - \frac{a^-}{\Delta X}\Psi^-_{i+3/2}\frac{(u_{i+2} - u_{i+1})}{2}, \tag{14}$$

where $\Psi^+_{i+1/2}$, $\Psi^-_{i+1/2}$ are the so-called flux limiters. Setting $\Psi^\pm_j = 1$ for all $j$ in (14) clearly recovers (12). Notice that, if

$$\Psi^\pm_{i+1/2} = 1 + \mathcal{O}(\Delta X) \tag{15}$$

the numerical approximation (14) is still second-order accurate. Indeed, define the so-called antidiffusive flux

$$\frac{f^{\text{high}}_{i+1/2} - f^{\text{high}}_{i-1/2}}{\Delta X} - \frac{f^{\text{low}}_{i+1/2} - f^{\text{low}}_{i-1/2}}{\Delta X} = \frac{a^+}{\Delta X}\frac{(u_i - u_{i-1})}{2} - \frac{a^+}{\Delta X}\frac{(u_{i-1} - u_{i-2})}{2} + \frac{a^-}{\Delta X}\frac{(u_{i+1} - u_i)}{2} - \frac{a^-}{\Delta X}\frac{(u_{i+2} - u_{i+1})}{2}.$$

Then, it can be checked that the anti-diffusive flux is $\mathcal{O}(\Delta X)$ accurate, so that a second-order correction is introduced if (15) holds. Notice also that the first-order Roe scheme is recovered if $\Psi^\pm_{i+1/2} = 0$.

Away from local extrema of the computed solution, we can compute the ratios

$$\theta^+_{i+1/2} = \frac{u_{i+2} - u_{i+1}}{u_{i+1} - u_i}, \quad \theta^-_{i+1/2} = \frac{u_i - u_{i-1}}{u_{i+1} - u_i} \tag{16}$$

and rewrite (14) as

$$\left.\frac{\delta f}{\delta x}\right|_{x_i} = \frac{a^+}{\Delta x}\left[1 + \frac{1}{2}\Psi^+_{i-1/2} - \frac{1}{2}\frac{\Psi^+_{i-3/2}}{\theta^+_{i-3/2}}\right](u_i - u_{i-1}) + \frac{a^-}{\Delta x}\left[1 + \frac{1}{2}\Psi^-_{i+1/2} - \frac{1}{2}\frac{\Psi^-_{i+3/2}}{\theta^-_{i+3/2}}\right](u_{i+1} - u_i). \tag{17}$$

Setting

$$\Psi^+_{i+1/2} = \Psi\left(\theta^+_{i+1/2}\right), \quad \Psi^-_{i+1/2} = \Psi\left(\theta^-_{i+1/2}\right)$$

it can be shown (see [20]) that the scheme (13)–(17) is second-order accurate (away from local extrema) and TVD if the function $\Psi$ satisfies

$$\Psi(1) = 1 \tag{18}$$

and

$$\frac{\Psi(\theta)}{\theta} - \Psi(\sigma) \leqslant 2 \tag{19}$$

for all values of $\theta$ and $\sigma$. Notice that the function $\Psi$ works directly on the slopes of the unknown variables, and, actually, behaves as a slope limiter.

The discretization above is not well defined at the local extrema of the computed solution, where the ratios (16) are null or cannot be defined. To overcome this limitation, we shall set

$$\Psi^-_{i+1/2} = \Psi^+_{i+1/2} = \Psi^-_{i+3/2} = \Psi^+_{i-1/2} = 0$$

for those $i$ such that

$$u_{i+1} - u_i = 0.$$

By doing so, the accuracy of the method reduces to first-order near local extrema.

Let us now define the still unspecified flux limiting function $\Psi$. Among the several examples present in the literature, we consider the following functions, that will be denoted, for the sake of brevity, by SL1($\theta$), SL2($\theta$) and SL3($\theta$), respectively:

- the *minmod* limiter

$$\Psi(\theta) = \mathrm{SL1}(\theta) = \begin{cases} \min(\theta, 1) & \text{if } \theta > 0, \\ 0 & \text{if } \theta \leqslant 0 \end{cases}$$

- the limiter proposed by Van Albada et al. (see [22])

$$\Psi(\theta) = \mathrm{SL2}(\theta) = \frac{\theta^2 + \theta}{1 + \theta^2}$$

- the *Superbee* limiter

$$\Psi(\theta) = \mathrm{SL3}(\theta) = \max[0, \min(2\theta, 1), \min(\theta, 2)].$$

Finally, notice that by simply setting

$$\Psi(\theta) = 0$$

the scheme (13)–(17) reduces to the first-order Roe semidiscretization (see [21]).

### 3.2. The second-order scheme for the discretization of a hyperbolic system of conservation laws

In this section, we extend the second-order difference scheme illustrated in Section 3.1 to the discretization of the following nonlinear system of conservation laws

$$\frac{\partial \mathbf{U}}{\partial t} + \frac{\partial \mathbf{F}}{\partial x} = 0. \tag{20}$$

System (20) corresponds to the hyperbolic part of the hydrodynamic model (1) in one spatial dimension, provided that we set

$$\mathbf{U} = \begin{pmatrix} n \\ nu \\ ne \end{pmatrix}, \quad \mathbf{F} = \mathbf{F}(\mathbf{U}) = \begin{pmatrix} nu \\ nu^2 + nRT \\ nue + nuRT \end{pmatrix}.$$

Let $\mathbf{A}(\mathbf{U}) = \frac{\mathrm{d}}{\mathrm{d}\mathbf{U}}\mathbf{F}(\mathbf{U})$ be the Jacobian matrix of the vector of convective fluxes, and let $\mathbf{R}$ and $\mathrm{diag}(\lambda_1, \ldots, \lambda_p)$ be the eigenvector and eigenvalue matrices of $\mathbf{A}$, respectively, $p$ being the dimension of the vector of the unknowns. Moreover, we define

$$\lambda_h^{\pm} = \frac{1}{2}(\lambda_h \pm |\lambda_h|), \quad h = 1, \ldots, p, \tag{21}$$

$$\mathbf{\Lambda}^{\pm} = \mathrm{diag}(\lambda_1^{\pm}, \ldots, \lambda_p^{\pm}),$$

$$\mathbf{A}^{\pm} = \mathbf{R}\mathbf{\Lambda}^{\pm}\mathbf{R}^{-1}, \quad |\mathbf{A}| = \mathbf{A}^{+} - \mathbf{A}^{-}.$$

Let us consider the Roe Jacobian matrix $\mathbf{A}_{i+1/2} = \mathbf{A}(\mathbf{U}_{i+1/2})$ such that (see [21])

$$\mathbf{A}_{i+1/2}(\mathbf{U}_{i+1} - \mathbf{U}_i) = \mathbf{F}_{i+1} - \mathbf{F}_i$$

and let us define the characteristic increments

$$\Delta\mathbf{V}_{i+1/2} = \left[\Delta v_{1_{i+1/2}}, \ldots, \Delta v_{p_{i+1/2}}\right] = \mathbf{R}_{i+1/2}^{-1}\mathbf{\Delta}\mathbf{U}_{i+1/2},$$

where, for any vector $\mathbf{S}$, we denote by $\mathbf{\Delta}$ the difference operator

$$\mathbf{\Delta}\mathbf{S}_{i+1/2} = \mathbf{S}_{i+1} - \mathbf{S}_i.$$

We consider the second-order spatial discretization

$$\left.\frac{\partial \mathbf{F}}{\partial x}\right|_{x_i} \doteq \frac{1}{\Delta X}\left(\mathbf{F}_{i+1/2}^{\mathrm{high}} - \mathbf{F}_{i-1/2}^{\mathrm{high}}\right), \tag{22}$$

where the high-order fluxes

$$\mathbf{F}_{i+1/2}^{\mathrm{high}} = \frac{1}{2}(\mathbf{F}_i + \mathbf{F}_{i+1}) - \frac{1}{2}|\mathbf{A}|_{i+1/2}(\mathbf{U}_{i+1} - \mathbf{U}_i) + \frac{1}{2}\mathbf{A}_{i-1/2}^{+}(\mathbf{U}_i - \mathbf{U}_{i-1}) - \frac{1}{2}\mathbf{A}_{i+3/2}^{-}(\mathbf{U}_{i+2} - \mathbf{U}_{i+1}) \tag{23}$$

are evaluated starting from the low-order fluxes

$$\mathbf{F}_{i+1/2}^{\mathrm{low}} = \frac{1}{2}(\mathbf{F}_{i+1} + \mathbf{F}_i) - \frac{1}{2}|\mathbf{A}|_{i+1/2}(\mathbf{U}_{i+1} - \mathbf{U}_i) \tag{24}$$

and performing the fully one-side upwinded extrapolation

$$\mathbf{F}_{i+1/2}^{\mathrm{high}} = \mathbf{F}_{i+1/2}^{\mathrm{low}} + \frac{1}{2}\left(\mathbf{F}_i - \mathbf{F}_{i-1/2}^{\mathrm{low}}\right) + \frac{1}{2}\left(\mathbf{F}_{i+1} - \mathbf{F}_{i+3/2}^{\mathrm{low}}\right). \tag{25}$$

Clearly, (22)–(24) and (25) are the extension of (7), (8), (10) and (11) to the case of hyperbolic systems.

The scheme (22) and (23) can be rewritten as

$$\left.\frac{\partial \mathbf{F}}{\partial x}\right|_{x_i} \doteq \frac{1}{\Delta X}\left[\mathbf{A}_{i+1/2}^{-}(\mathbf{U}_{i+1} - \mathbf{U}_i) + \mathbf{A}_{i-1/2}^{+}(\mathbf{U}_i - \mathbf{U}_{i-1}) + \frac{1}{2}\mathbf{A}_{i-1/2}^{+}(\mathbf{U}_i - \mathbf{U}_{i-1}) - \frac{1}{2}\mathbf{A}_{i-3/2}^{+}(\mathbf{U}_{i-1} - \mathbf{U}_{i-2}) + \frac{1}{2}\mathbf{A}_{i+1/2}^{-}(\mathbf{U}_{i+1} - \mathbf{U}_i) - \frac{1}{2}\mathbf{A}_{i+3/2}^{-}(\mathbf{U}_{i+2} - \mathbf{U}_{i+1})\right],$$

which is the counterpart of (12) in the case of hyperbolic systems.

As in the scalar case, in order to make the scheme TVD, we replace the expression above with

$$\left.\frac{\partial \mathbf{F}}{\partial x}\right|_{x_i} \doteq \frac{1}{\Delta X}\left[\mathbf{A}^-_{i+1/2}(\mathbf{U}_{i+1}-\mathbf{U}_i)+\mathbf{A}^+_{i-1/2}(\mathbf{U}_i-\mathbf{U}_{i-1})+\frac{1}{2}\mathbf{\Phi}^+_{i-1/2}\mathbf{A}^+_{i-1/2}(\mathbf{U}_i-\mathbf{U}_{i-1})\right.$$
$$\left.-\frac{1}{2}\mathbf{\Pi}^+_{i-3/2}\mathbf{A}^+_{i-3/2}(\mathbf{U}_{i-1}-\mathbf{U}_{i-2})+\frac{1}{2}\mathbf{\Phi}^-_{i+1/2}\mathbf{A}^-_{i+1/2}(\mathbf{U}_{i+1}-\mathbf{U}_i)-\frac{1}{2}\mathbf{\Pi}^-_{i+3/2}\mathbf{A}^-_{i+3/2}(\mathbf{U}_{i+2}-\mathbf{U}_{i+1})\right], \tag{26}$$

where $\mathbf{\Phi}^{\pm}_{i+1/2}$, $\mathbf{\Pi}^{\pm}_{i+3/2}$ are suitable matrices of flux limiters, that must be equal, up to $\mathcal{O}(\Delta X)$ terms, to the identity matrix, in presence of regular solutions and for almost all the nodes of the mesh. Clearly, (26) is the extension of (14) to the case of hyperbolic systems.

Now, by directly limiting the slopes of the characteristic variables, we want to get a TVD scheme when applied to nonlinear hyperbolic equations and to linear hyperbolic systems with constant coefficients. With this aim, for $h = 1,\ldots,p$, let us define the quantities

$$\omega^-_{h_{i+1/2}} = \frac{\Delta v_{h_{i+1/2}}}{\Delta v_{h_{i-1/2}}}, \quad \omega^+_{h_{i+1/2}} = \frac{\Delta v_{h_{i+1/2}}}{\Delta v_{h_{i+3/2}}},$$

$$\theta^-_{h_{i+1/2}} = \frac{\Delta v_{h_{i-1/2}}}{\Delta v_{h_{i+1/2}}}, \quad \theta^+_{h_{i+1/2}} = \frac{\Delta v_{h_{i+3/2}}}{\Delta v_{h_{i+1/2}}},$$

$$\psi^-_{h_{i+1/2}} = \Psi\left(\theta^-_{h_{i+1/2}}\right), \quad \psi^+_{h_{i+1/2}} = \Psi\left(\theta^+_{h_{i+1/2}}\right),$$

$$\xi^-_{h_{i+1/2}} = \begin{cases} \dfrac{\lambda^-_{h_{i-1/2}}}{\lambda^-_{h_{i+1/2}}} & \text{if } \lambda^-_{h_{i+1/2}} \neq 0, \\ 1 & \text{if } \lambda^-_{h_{i+1/2}} = 0, \end{cases}$$

$$\xi^+_{h_{i+1/2}} = \begin{cases} \dfrac{\lambda^+_{h_{i+3/2}}}{\lambda^+_{h_{i+1/2}}} & \text{if } \lambda^+_{h_{i+1/2}} \neq 0, \\ 1 & \text{if } \lambda^+_{h_{i+1/2}} = 0, \end{cases}$$

where $\Psi$ is the flux limiting function defined in Section 3.1. Moreover, let us introduce the diagonal matrices

$$\mathbf{\Omega}^{\pm}_{i+1/2} = \operatorname{diag}\left(\omega^{\pm}_{1_{i+1/2}},\ldots,\omega^{\pm}_{p_{i+1/2}}\right), \quad \mathbf{\Theta}^{\pm}_{i+1/2} = \operatorname{diag}\left(\theta^{\pm}_{1_{i+1/2}},\ldots,\theta^{\pm}_{p_{i+1/2}}\right),$$

$$\mathbf{\Psi}^{\pm}_{i+1/2} = \operatorname{diag}\left(\psi^{\pm}_{1_{i+1/2}},\ldots,\psi^{\pm}_{p_{i+1/2}}\right), \quad \mathbf{\Xi}^{\pm}_{i+1/2} = \operatorname{diag}\left(\xi^{\pm}_{1_{i+1/2}},\ldots,\xi^{\pm}_{p_{i+1/2}}\right).$$

Now, in order to obtain a scheme that is second-order accurate and TVD along the characteristic directions, we set

$$\mathbf{\Phi}^-_{i+1/2} = \mathbf{R}_{i+1/2}\mathbf{\Psi}^-_{i+1/2}\mathbf{R}^{-1}_{i+1/2}, \tag{27}$$

$$\mathbf{\Pi}^-_{i+3/2} = \mathbf{R}_{i+3/2}\mathbf{\Psi}^-_{i+3/2}\mathbf{\Omega}^-_{i+3/2}\mathbf{R}^{-1}_{i+3/2}\mathbf{R}_{i+1/2}\mathbf{\Xi}^-_{i+3/2}\mathbf{\Theta}^-_{i+3/2}\mathbf{R}^{-1}_{i+3/2}, \tag{28}$$

$$\mathbf{\Phi}^{+}_{i-1/2} = \mathbf{R}_{i-1/2}\mathbf{\Psi}^{+}_{i-1/2}\mathbf{R}^{-1}_{i-1/2}, \tag{29}$$

$$\mathbf{\Pi}^{+}_{i-3/2} = \mathbf{R}_{i-3/2}\mathbf{\Psi}^{+}_{i-3/2}\mathbf{\Omega}^{+}_{i-3/2}\mathbf{R}^{-1}_{i-3/2}\mathbf{R}_{i-1/2}\mathbf{\Xi}^{+}_{i-3/2}\mathbf{\Theta}^{+}_{i-3/2}\mathbf{R}^{-1}_{i-3/2}. \tag{30}$$

Substituting (27)–(30) into (26), we get after some elementary matrix calculations the desired second-order TVD spatial discretization of the flux derivative

$$\begin{aligned}\left.\frac{\partial \mathbf{F}}{\partial x}\right|_{x_i} \doteq \frac{1}{\Delta X}\Bigg[&\mathbf{A}^{-}_{i+1/2}(\mathbf{U}_{i+1}-\mathbf{U}_i) + \mathbf{A}^{+}_{i-1/2}(\mathbf{U}_i-\mathbf{U}_{i-1}) \\ &\frac{1}{2}\mathbf{R}_{i-1/2}\mathbf{\Psi}^{+}_{i-1/2}\mathbf{R}^{-1}_{i-1/2}\mathbf{A}^{+}_{i-1/2}(\mathbf{U}_i-\mathbf{U}_{i-1}) \\ &-\frac{1}{2}\mathbf{R}_{i-3/2}\mathbf{\Psi}^{+}_{i-3/2}\mathbf{\Omega}^{+}_{i-3/2}\mathbf{R}^{-1}_{i-3/2}\mathbf{A}^{+}_{i-1/2}(\mathbf{U}_i-\mathbf{U}_{i-1}) + \frac{1}{2}\mathbf{R}_{i+1/2}\mathbf{\Psi}^{-}_{i+1/2}\mathbf{R}^{-1}_{i+1/2}\mathbf{A}^{-}_{i+1/2}(\mathbf{U}_{i+1}-\mathbf{U}_i) \\ &-\frac{1}{2}\mathbf{R}_{i+3/2}\mathbf{\Psi}^{-}_{i+3/2}\mathbf{\Omega}^{-}_{i+3/2}\mathbf{R}^{-1}_{i+3/2}\mathbf{A}^{-}_{i+1/2}(\mathbf{U}_{i+1}-\mathbf{U}_i)\Bigg]\end{aligned} \tag{31}$$

that can be written in the following compact form

$$\begin{aligned}\left.\frac{\partial \mathbf{F}}{\partial x}\right|_{x_i} \equiv \left.\frac{\delta \mathbf{F}}{\delta x}\right|_{x_i} \doteq &\frac{1}{\Delta X}\left[\mathbf{I}+\frac{1}{2}\mathbf{R}_{i-1/2}\mathbf{\Psi}^{+}_{i-1/2}\mathbf{R}^{-1}_{i-1/2}-\frac{1}{2}\mathbf{R}_{i-3/2}\mathbf{\Psi}^{+}_{i-3/2}\mathbf{\Omega}^{+}_{i-3/2}\mathbf{R}^{-1}_{i-3/2}\right]\left(\mathbf{F}_i-\mathbf{F}^{\text{low}}_{i-1/2}\right) \\ &+\frac{1}{\Delta X}\left[\mathbf{I}+\frac{1}{2}\mathbf{R}_{i+1/2}\mathbf{\Psi}^{-}_{i+1/2}\mathbf{R}^{-1}_{i+1/2}-\frac{1}{2}\mathbf{R}_{i+3/2}\mathbf{\Psi}^{-}_{i+3/2}\mathbf{\Omega}^{-}_{i+3/2}\mathbf{R}^{-1}_{i+3/2}\right]\left(\mathbf{F}^{\text{low}}_{i+1/2}-\mathbf{F}_i\right).\end{aligned} \tag{32}$$

For those $i$ where some of the entries in the vector $\Delta\mathbf{V}_{i+1/2}$ vanish, the matrices $\mathbf{\Psi}^{\pm}_{i+1/2}$, $\mathbf{\Psi}^{+}_{i-3/2}$, $\mathbf{\Psi}^{-}_{i+3/2}$, $\mathbf{\Omega}^{\pm}_{i+1/2}$, $\mathbf{\Omega}^{+}_{i-3/2}$, $\mathbf{\Omega}^{-}_{i+3/2}$ cannot be constructed by the procedure above. As in the scalar case, the procedure to overcome this problem consists of setting to zero the entries of such matrices that cannot be computed due to division by zero.

Let us now discretize the time derivatives in (20) using the forward Euler scheme, and consider the fully discrete approximation

$$\frac{\mathbf{U}^{k+1}_i-\mathbf{U}^{k}_i}{\Delta t} + \left.\frac{\delta \mathbf{F}}{\delta x}\right|^{k}_{x_i} = \mathbf{0}, \tag{33}$$

where $\left.\frac{\delta \mathbf{F}}{\delta x}\right|^{k}_{x_i}$ is computed at each time level $t_k$ according to relation (32).

**Proposition 1.** *When applied to linear hyperbolic systems with constant matrix* $\mathbf{A}$ *the numerical scheme* (32), (33) *is* TVD *along the characteristic directions.*

**Proof.** It is enough to notice that taking the product to the left of Eqs. (32), (33) with the constant eigenvector matrix $\mathbf{R}$ leads to the TVD formulation (13)–(17) in each characteristic variable. Notice also that Proposition 1 holds true also for nonlinear hyperbolic systems with constant characteristic directions. □

**Proposition 2.** *The numerical scheme* (32), (33) *applied to nonlinear scalar conservation laws is* TVD.

**Proof.** The result immediately follows by noticing that relation (32) degenerates, in the scalar case, into the form (17) that can be proved to be TVD (see [20]). □

**Proposition 3.** *Away from local extrema, in presence of a regular solution and choosing a sufficiently smooth function* $\Psi$, *the spatial semi-discretization* (31) *is second-order accurate.*

**Proof.** The proof immediately follows from the fact that the quantities $\mathbf{\Phi}^{-}_{i+1/2}$, $\mathbf{\Pi}^{-}_{i+3/2}$, $\mathbf{\Phi}^{+}_{i-1/2}$ and $\mathbf{\Pi}^{+}_{i-3/2}$, due to the consistency requirement (18), are first-order approximations of the identity matrix, away from local extrema of the characteristic variables. On the other hand, at local extrema, it can be shown that the numerical scheme reduces to first-order. □

**Remark 3.1.** We explicitly point out that, since the time derivatives in (20) are discretized by the forward Euler scheme, the second-order accuracy of the numerical method must be intended in space, only.

**Remark 3.2.** It is well known that the numerical solutions computed by the Roe scheme may exhibit nonphysical expansion shocks, due to the small amount of artificial viscosity introduced near sonic points. To avoid this problem, we modify the low-order fluxes in (32) using the entropy correction proposed by Harten [18], that consists of evaluating the matrices $\mathbf{\Lambda}^{\pm}$ as

$$\mathbf{\Lambda}^{\pm} = \frac{\mathbf{\Lambda} \pm \mathbf{Q}}{2},$$

where $\mathbf{Q}$ is the diagonal matrix

$$\mathbf{Q}_{h,h} = \begin{cases} |\lambda_h| & \text{if } |\lambda_h| \geqslant 2\rho, \\ \dfrac{\lambda_h^2}{4\rho} + \rho & \text{if } |\lambda_h| < 2\rho \end{cases} \tag{34}$$

$\rho$ being a given tolerance. In the numerical experiments we take $\rho = 0.05c_0$, where $c_0 = \sqrt{5RT_0/3}$ is the speed of sound at thermodynamic equilibrium.

**Remark 3.3.** For the numerical approximation of the remaining spatial differential terms, namely, the divergence of the electric field in (2), the gradient of the electrostatic potential in (3) and the divergence of the heat flux in the energy equation, the usual centered finite difference approximation is employed. Moreover, in order to enhance the stability of the numerical scheme, the semi-implicit time discretization of the relaxation terms

$$\frac{n\mathbf{v}}{\tau_p} \doteq \frac{n^{k+1}\mathbf{v}^{k+1}}{\tau_p^k}, \quad \frac{ne - ne_0}{\tau_w} \doteq \frac{n^{k+1}e^{k+1} - n^{k+1}e_0}{\tau_w^k}$$

is performed without any additional computational effort (the relaxation terms having a diagonal form in the hydrodynamic system (1)).

## 4. Numerical results

This section is devoted to the discussion of the numerical results obtained in the simulation of a submicron $n^+ - n - n^+$ diode in the one-dimensional case. Namely, we study a 0.6 μm silicon diode with 0.1 μm source, 0.4 μm channel and 0.1 μm drain.

In our experiments, we have used the following quantities (which are similar to those in [16]): $m = 0.26m_e$, $m_e$ being the free electron mass, $\epsilon = 11.7\epsilon_0$, $\epsilon_0$ being the vacuum dielectric permittivity, and $N_{ref} = 1.44 \times 10^{21}$ m$^{-3}$, $\alpha = 0.659$, $v_s = 1.2 \times 10^5$ m s$^{-1}$, $\Delta\mu = 1.8$.

The device doping profile is defined as follows:

$$N(x) = \begin{cases} 5 \times 10^{23} \text{ m}^{-3} & \text{if } 0 \leqslant x \leqslant 0.1 \text{ μm or } 0.5 \leqslant x \leqslant 0.6 \text{ μm}, \\ 1 \times 10^{21} \text{ m}^{-3} & \text{if } 0.1 < x < 0.5 \text{ μm}. \end{cases} \tag{35}$$

Appropriate boundary conditions are (see [16]):

- at the source ($x = 0$): $n = N(0)$, $T = T_0$, $\phi = \phi_{\text{built-in}}$
- at the drain ($x = L_{\text{Tot}}$): $n = N(L_{\text{Tot}})$, $T = T_0$, $\phi = \phi_{\text{built-in}} + \phi_{\text{bias}}$

where $\phi_{\text{built-in}} = (K_B T_0/q_n)\log(N(0)/n_i)$ is the built-in voltage arising between the semiconductor and the metal contact and $n_i$ is the intrinsic concentration in the semiconductor. As in [16], we have used $n_i = 2.84 \times 10^{-14}$ m$^{-3}$.

In all the numerical experiments, the lattice temperature is $T_0 = 77$ K and the applied biasing potential is $\phi_{\text{bias}} = 2$ V. It is well known that at such a working temperature electron flow is supersonic and shock waves are experienced by the electron density, velocity and temperature distributions (see [7–9,16]).

At $t = 0$ we set $u = 0$ and $T = T_0$. In order to investigate the influence of the smoothness of the initial electron concentration on the convergence of the numerical scheme, at $t = 0$ we set

$$n(x) = \begin{cases} 5 \times 10^{23} \text{ m}^{-3} & \text{if } 0 \leqslant x \leqslant 0.1 \text{ μm or } 0.5 \leqslant x \leqslant 0.6 \text{ μm}, \\ 1 \times 10^{21} \text{ m}^{-3} & \text{if } 0.1 + \delta \leqslant x \leqslant 0.5 - \delta \text{ μm} \end{cases} \tag{36}$$

and we connect the above piecewise constant values by a $C^1$ smooth cosine law. Notice that, according to (36), the initial electron profile is equal to the doping concentration on all the semiconductor device except on two intervals of length equal to $\delta$, where the jumps at the junctions of the initial electron density are smeared out. We have performed a parametric study on $\delta$ in the range $[0, 0.15$ μm$]$. As we will see, this parameter, measuring the regularity of the initial solution, can strongly affect the convergence of the numerical method.

We remark that a similar analysis has been performed on the abruptness of the doping profile, where the function (35) has been regularized with smooth cosine connection as follows

$$N(x) = \begin{cases} 5 \times 10^{23} \text{ m}^{-3} & \text{if } 0 \leqslant x \leqslant 0.1 \text{ μm or } 0.5 \leqslant x \leqslant 0.6 \text{ μm}, \\ 1 \times 10^{21} \text{ m}^{-3} & \text{if } 0.1 + \delta < x < 0.5 - \delta \text{ μm}. \end{cases}$$

However, the numerical experiments have revealed that choosing $\delta$ in the range [0,0.15 μm] does not influence the properties of the discretization scheme. As a conclusion, the convergence of the numerical method is affected by the jump of the doping density (which determines the strength of the electric field at the junctions), but not by the abruptness of such variations.

In order to investigate the influence of the regularity of the solution on the stability of the numerical scheme proposed in Section 3, different values of the quantities $k_{\text{W-F}}$ and $\delta$ are used in the simulations, according to the following schedule:

- Test case 1: $k_{\text{W-F}} = 0$, $\delta = 0$.
- Test case 2: $k_{\text{W-F}} = 0$, $\delta = 0.1$ μm.
- Test case 3: $k_{\text{W-F}} = 0$, $\delta = 0.15$ μm.
- Test case 4: $k_{\text{W-F}} = 0.2$, $\delta = 0$ μm.
- Test case 5: $k_{\text{W-F}} = 0.2$, $\delta = 0.1$ μm.

In the numerical experiments, all of the three slope limiters SL1, SL2 and SL3 introduced in Section 3 are employed. Computations have also been performed using the Roe first-order approximation, corresponding to taking $\Psi = 0$. The quantity $N_x$ denotes the number of spatial nodes ($N_x = 200$ and $N_x = 400$ in all of the examples). The experiments show situations in which the steady state is not reached. Concerning this point, Tables 1–5 illustrate, for each test case, if the numerical method converges or fails to converge ('conv' and 'no conv' indicates convergence and failure to convergence, respectively).

As we can see, the first-order scheme does reach convergence in all of the experiments, while the second-order scheme, in some situations, does not. We have experienced in all the simulations, in correspondence of convergence breakdown, the following behaviour of the computed solution: during the transient to steady state, the solution is non-monotone, and the conservative variables **U** are affected by spurious

Table 1
Test case 1

| | $\Psi(\theta) = 0$ | $\Psi(\theta) = \mathrm{SL1}(\theta)$ | $\Psi(\theta) = \mathrm{SL2}(\theta)$ | $\Psi(\theta) = \mathrm{SL3}(\theta)$ |
|---|---|---|---|---|
| $N_x = 200$ | Conv | No conv | No conv | No conv |
| $N_x = 400$ | Conv | No conv | No conv | No conv |

Table 2
Test case 2

| | $\Psi(\theta) = 0$ | $\Psi(\theta) = \mathrm{SL1}(\theta)$ | $\Psi(\theta) = \mathrm{SL2}(\theta)$ | $\Psi(\theta) = \mathrm{SL3}(\theta)$ |
|---|---|---|---|---|
| $N_x = 200$ | Conv | No conv | No conv | No conv |
| $N_x = 400$ | Conv | No conv | No conv | No conv |

Table 3
Test case 3

| | $\Psi(\theta) = 0$ | $\Psi(\theta) = \mathrm{SL1}(\theta)$ | $\Psi(\theta) = \mathrm{SL2}(\theta)$ | $\Psi(\theta) = \mathrm{SL3}(\theta)$ |
|---|---|---|---|---|
| $N_x = 200$ | Conv | Conv | Conv | No conv |
| $N_x = 400$ | Conv | Conv | Conv | No conv |

Table 4
Test case 4

| | $\Psi(\theta) = 0$ | $\Psi(\theta) = \mathrm{SL1}(\theta)$ | $\Psi(\theta) = \mathrm{SL2}(\theta)$ | $\Psi(\theta) = \mathrm{SL3}(\theta)$ |
|---|---|---|---|---|
| $N_x = 200$ | Conv | Conv | Conv | No conv |
| $N_x = 400$ | Conv | Conv | Conv | Conv |

Table 5
Test case 5

| | $\Psi(\theta) = 0$ | $\Psi(\theta) = \mathrm{SL1}(\theta)$ | $\Psi(\theta) = \mathrm{SL2}(\theta)$ | $\Psi(\theta) = \mathrm{SL3}(\theta)$ |
|---|---|---|---|---|
| $N_x = 200$ | Conv | Conv | Conv | Conv |
| $N_x = 400$ | Conv | Conv | Conv | Conv |

oscillations at the drain junction (see Figs. 1 and 2). The oscillations make the electron density (shown in Fig. 2), become negative, so that also the electron temperature becomes negative, and the numerical simulation stops.

Some remarks are here in order:

1. Reducing the time integration does not change the behaviour described above. To assess the validity of this statement, we have used values of $\Delta t$ up to 1000 times smaller than the time step at which the first-order approximation works, but the numerical instability has not been removed. On the contrary, once the space interval $\Delta X$ is fixed, the instability occurs always at the same time, that is not influenced by the value of $\Delta t$.
2. Failure to convergence is influenced by the spatial discretization. To see this point, we have carried out a numerical simulation of Test case 1 (choosing the slope limiter SL1) on a very refined mesh of 2000 nodes

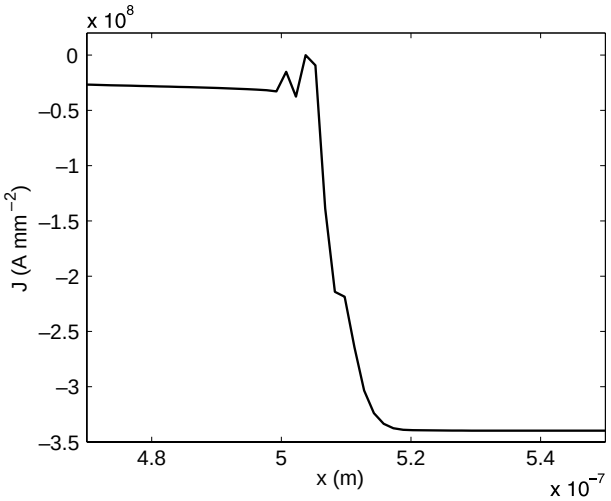


Fig. 1. Test case 1, with slope limiter SL1 and $N_x = 400$: electron current at $t = 1.86$ ps, zoom at the drain junction.

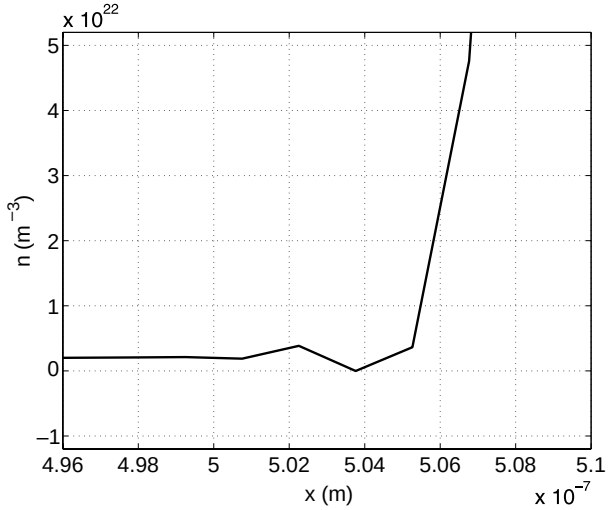


Fig. 2. Test case 1, with slope limiter SL1 and $N_x = 400$: electron density at $t = 1.86$ ps, zoom at the drain junction.

($N_x = 2000$), and the steady state has been reached. This seems to suggest that failing to converge does not necessarily indicate the lack of an analytical solution to the hydrodynamic system of equations (we have performed only one simulation using 2000 spatial nodes, since the computational cost of working with such a refined mesh is very expensive).

The fact that the computed solution is affected by spurious oscillations reveals that the numerical method is *actually* not TVD. Indeed, as already pointed out in Section 3, the scheme can achieve total variation diminishing only in the case where the characteristic directions (the eigenvectors **R**) are constant. Now, at the drain junction of the device, the solution experiences very strong variations, due to the presence

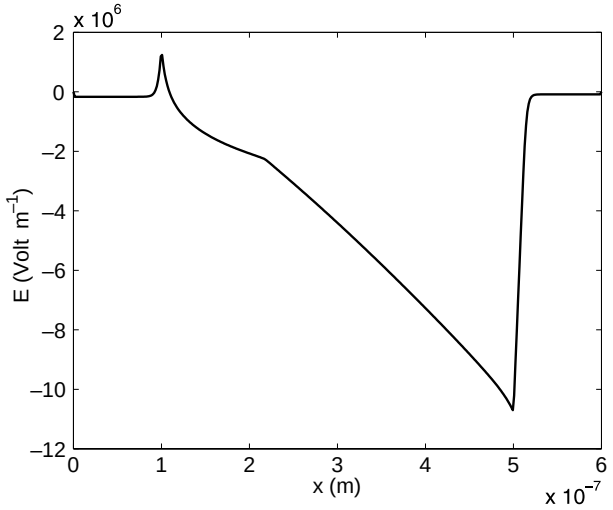


Fig. 3. Test case 1, 2, 3, with slope limiter SL1 and $N_x = 400$: electric field at steady state.

of a high electric field (see Fig. 3), and the characteristic directions are far from being constant. For this reason, some spurious oscillations occur, and their amplitude, despite being moderate, is large enough to make the electron concentration, which is small at the end of the channel, become negative, thus yielding the numerical instability. Comparing Tables 1–3, we notice that the method achieves better stability when the regularity of the initial solution increases. This can be explained by the fact that, when the solution is smoother, the characteristic directions tend to become constant on adjacent grid points, leading to 'a more TVD' approximation. The same argument can be applied to explain why the stability of the method can be improved by increasing the number of nodes of the mesh.

We remark that a 'monotonicity improvement' of the steady electron current due to grid refinement has also been observed in [17].

Numerical stability can also be enhanced by increasing the amount of heat dissipation present in the physical model (see Tables 4 and 5). This is not surprising since, in such a case, we are adding a diffusive and regularizing contribution to the whole set of equations.

Concerning the influence of the choice of the flux limiter on the numerical stability, it is worth noticing in Tables 1–5 that SL1 and SL2 exhibit the same behaviour, while SL3, looking at Test cases 4 and 5, reveals to be more unstable. This can be explained by the fact that the function SL3 actually coincides with the boundary of the region where the approximation is TVD, i.e. if $\Psi(\theta) > \mathrm{SL3}(\theta)$, then the discretization is no longer total variation diminishing (see [20]). For this reason, the attitude of the numerical method to become non TVD, and to generate oscillations, in the nonlinear regime is greater when SL3 is used rather than SL1 or SL2.

Let us now investigate the spatial accuracy of the numerical method. First of all, we point out that the main difference between the second-order scheme and the first-order one concerns the approximation of the electron current, which is, among the physical quantities, the most sensitive to numerical errors, as already shown in [3,15]. For instance, as we can see in Fig. 4, the second-order approximation of the steady electron velocity and the first-order one are almost the same, while the steady electron current profile is very sensitive to the order of approximation used.

In particular, Fig. 5 shows that the steady electron current profile is affected by wide oscillations at the drain junction of the device when the second-order scheme is used, experiencing also a jump there. Since the

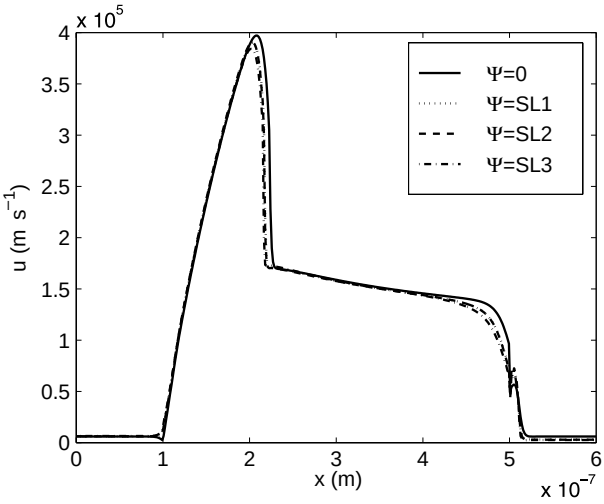


Fig. 4. Test case 4, 5: electron velocity at steady state.

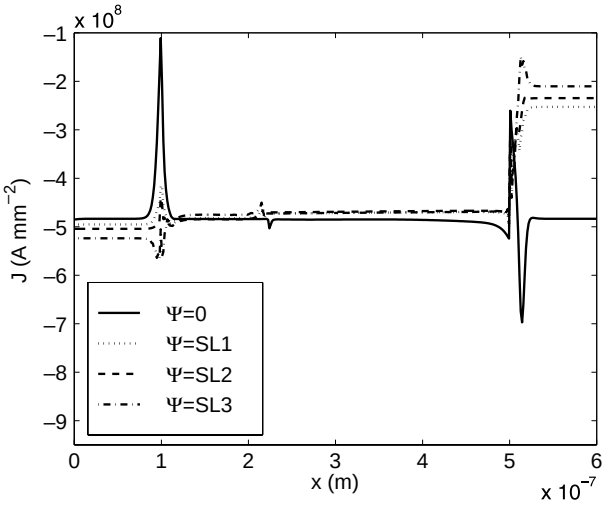


Fig. 5. Test case 4, 5: electron current at steady state.

electron current must be a constant function at steady state, the amplitude of the spurious oscillations and of the corresponding jump can be assumed as a measure of the numerical error. As already observed in [15], the deviation of the steady electron current from its mean value is quite relevant, and decreases after mesh refinement. However, the numerical experiments show that the error is reduced only by a factor of one half when the number of nodes is multiplied by two (see Fig. 6), which implies that the numerical method is first-order accurate at the drain junction of the semiconductor device. We remark that the electron current profile computed at steady state suffers the same loss of accuracy when the slope limiters SL1, SL2 and SL3 are used.

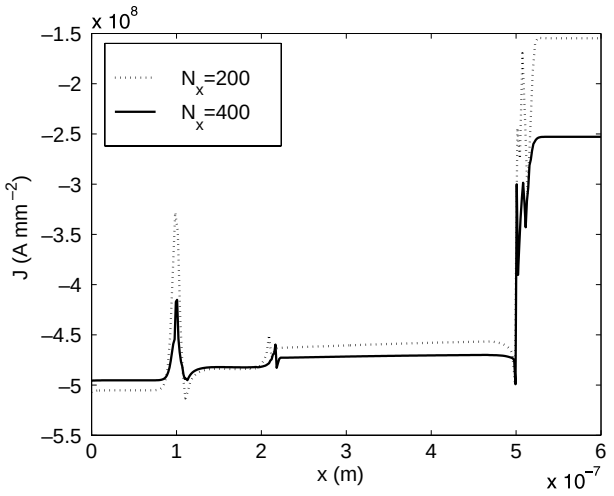


Fig. 6. Test case 4, 5, with slope limiter SL1: electron current at steady state.

A closer look at numerical results explains the inaccuracy of the high-order approximation: at the drain junction the slope limiters, which should counterbalance the large sources of error due to the strong variations of the solution, actually perform quite poorly. Let us denote by $\Psi_1$, $\Psi_2$, and $\Psi_3$ the slope limiters acting on the characteristic increments $\Delta v_1$, $\Delta v_2$, $\Delta v_3$, associated with the eigenvalues $\lambda_1 = u - c$, $\lambda_2 = u + c$ and $\lambda_3 = u$ respectively, $c = \sqrt{5RT/3}$ being the speed of sound in the device (since the flow at the end of the channel is subsonic only $\Psi_1^-$, $\Psi_2^+$, $\Psi_3^+$ matter).

Figs. 7–9 show the profiles of the slope limiters at the drain junction, obtained, at steady state, using SL1 (the choice of SL2 or SL3 would give similar results). As we can notice, the functions $\Psi_1$ and $\Psi_2$ are quite far from 1, and, moreover, they are not $1 + \mathcal{O}(\Delta X)$ since at the end of the channel the Riemann invariants

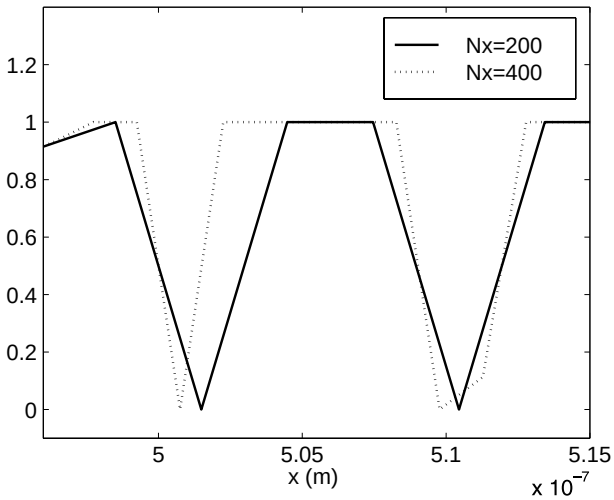


Fig. 7. Test case 4, 5, with slope limiter SL1: function $\Psi_1$ at steady state, zoom at the drain junction.

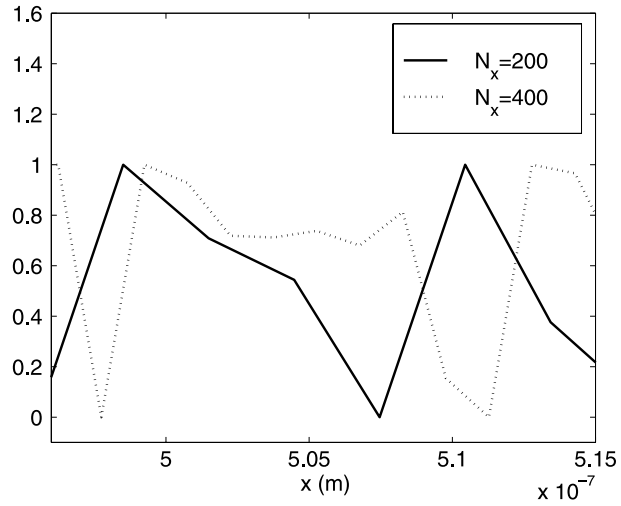


Fig. 8. Test case 4, 5, with slope limiter SL1: function $\Psi_2$ at steady state, zoom at the drain junction.

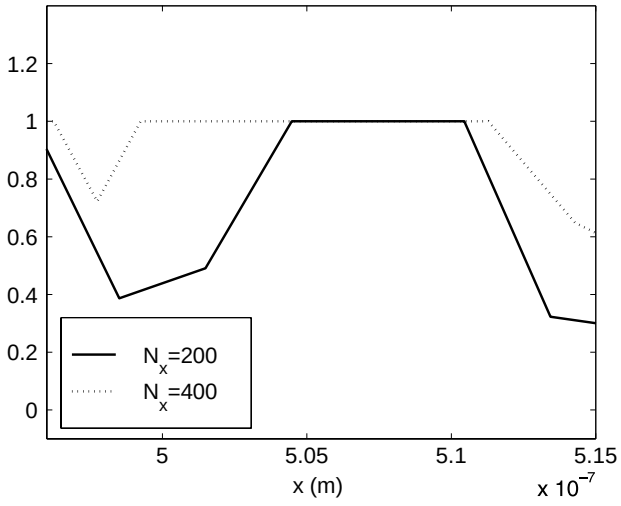


Fig. 9. Test case 4, 5, with slope limiter SL1: function $\Psi_3$ at steady state, zoom at the drain junction.

$v_1$, $v_2$ associated with the hyperbolic part of the hydrodynamic model and computed as the discrete summation of the characteristic increments $\Delta v_1$, $\Delta v_2$ exhibit, at steady state, two local extrema (see Figs. 10 and 11). Near these points, the ratio between two consecutive increments of $\Delta v_1$ and $\Delta v_2$ cannot be $1 + \mathcal{O}(\Delta X)$, and the slope limiters evaluated accordingly are not $1 + \mathcal{O}(\Delta X)$ as well.

Fig. 9 shows that, unlike in the case of $\Psi_1$ and $\Psi_2$, the function $\Psi_3$ is indeed $1 + \mathcal{O}(\Delta X)$, due to the fact that the discrete Riemann invariant $v_3$ (shown in Fig. 12) has no local extrema at the drain junction (actually $v_3$ exhibits a minimum before the end of the channel, but this is not a relevant source of error since the solution does not attain significant variations there). We point out that a local extremum (a minimum)

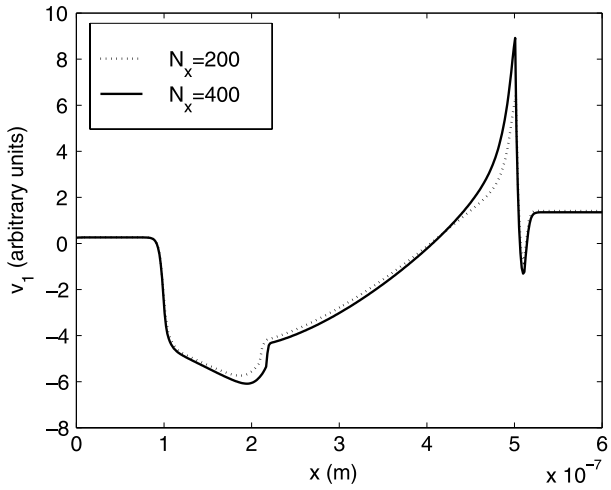


Fig. 10. Test case 4, 5: discrete Riemann invariant $v_1$, steady state.

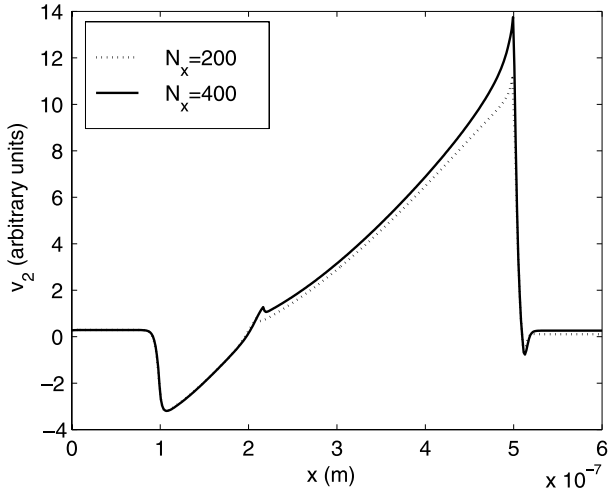


Fig. 11. Test case 4, 5: discrete Riemann invariant $v_2$, steady state.

is experienced by function $v_1$ also at the source junction where the electron current profile is affected by some $\mathcal{O}(\Delta X)$ oscillations as well.

As for the computation of shock wave in the electron velocity profile, we can notice that the high-order scheme produces a satisfactory approximation of the shock that is generated at steady-state at $x = 2.25$ μm, both in terms of resolution of the discontinuity (see Fig. 4) and of electron current conservation (see Fig. 5).

Finally, we do mention that, in all the experiments, the numerical solution is affected very weakly by the entropy correction (34). Indeed such an enforcement is effective only at sonic points, so it does not remove the numerical instabilities, and does not produce any relevant changes on the computed solution.

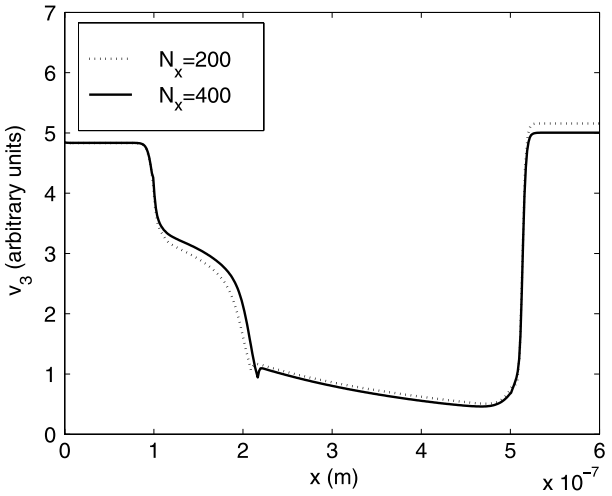


Fig. 12. Test case 4, 5: discrete Riemann invariant $v_3$, steady state.

## 5. Conclusions

In this paper, the hydrodynamic model for semiconductors is solved by a TVD second-order upwinded finite difference scheme. In particular, the high-order fluxes are evaluated by a fully upwinded extrapolation on adjacent cells of the first-order fluxes of Roe, allowing the semi-implicit discretization of the relaxation terms. Suitable TVD properties are then achieved by limiting the slopes of the discrete solution along the directions associated with the characteristics of the hyperbolic system.

The numerical simulation is carried out on the one-dimensional $n^+ - n - n^+$ diode benchmark problem, and several slope limiters are employed and compared, namely, the *minmod* function (SL1), the slope limiter of Van Albada (SL2) and the *superbee* limiter (SL3), together with the Roe first-order approximation scheme, corresponding to taking $\Psi = 0$.

Several test cases are numerically solved in order to investigate the convergence of the numerical method as a function of the smoothness of the solution of the hydrodynamical problem. In particular, it is shown that the scheme, being TVD only when applied to hyperbolic systems with constant characteristic directions, does not completely preserve the monotonicity of the discrete solutions. On the contrary, some spurious oscillations arise, which, despite being of moderate amplitude, can lead to convergence breakdown by making the electron density become negative.

The numerical instabilities are experienced in correspondence of strong variations of the computed solutions, and do not occur if the initial electron concentration is a smooth enough function. This gives a strong indication on a proper choice of the initial solution when the hydrodynamic model is applied to the simulation of more complex and multidimensional devices.

The experiments reveal that the spurious oscillations can also be controlled by suitably reducing the size of the computational grid, a phenomenon that we heuristically explain by the following argument: on a very refined grid, the characteristic directions of the hyperbolic system can be considered to be constant on adjacent mesh points, leading to a 'more TVD behaviour' of the numerical approximation (see Proposition 1).

A further control on the numerical instabilities can also be achieved by increasing the amount of heat conductivity present in the physical model, a fact that does not surprise, as we are adding a regularizing contribution to the whole set of the equations.

Concerning the influence of the choice of the slope limiter on the convergence of the method, it is interesting to notice that SL3 is more unstable than SL1 and SL2, since the *superbee* limiter coincides with the boundary of the TVD region of the numerical scheme, hence it is more sensitive to escaping from it in the strongly non-linear regime.

Finally, we remark that the first-order scheme reveals to be capable of reaching convergence to steady state in all of the numerical experiments.

As for the accuracy of the numerical method, the simulation results highlight that the electron current profile is non-monotone both at the source and the drain junction of the device. In particular, the spurious oscillations become very large at the drain end of the channel, where the computed electron current profile is not flat at steady state, but exhibits significant variations from the mean value, thus suffering a considerable loss of accuracy. The simulations reveal that such a numerical error can be reduced by mesh refinement, but it is $\mathcal{O}(\Delta X)$ only. This phenomenon is due to the poor behaviour of the flux limiters, that are quite significantly far from 1 at the drain junction, thus spoiling the performance of the high-order scheme in a spatial region where the solution experiences steep gradients and therefore the discretization error is relevant.

The experiments show also that the poor convergence of the flux limiters is related to the shape of the Riemann invariants of the hyperbolic part of the hydrodynamic set of equations, whose slopes are used to limit the anti-diffusive high-order fluxes. In particular, the Riemann invariants associated with the eigenvalues $u - c$ and $u + c$ have two points of local extremum at the end of the channel, causing the corresponding slope limiters be not $1 + \mathcal{O}(\Delta X)$ there.

Concerning this latter point, we notice that the same argument could be used to explain the considerable loss of accuracy on the steady electron current at the drain junction that is experienced by Anile and coworkers [3–5], where an extended hydrodynamic model taking into account the first five moments of the Boltzmann equations is solved by the Nessyahu–Tadmor scheme: in this case the slope limiters act directly on the primitive variables $\mathbf{U}$, and, looking at the results presented in the above works, at least two functions in the set $\mathbf{U}$, the electron energy and the heat flux, exhibit points of local extrema at the end of the channel at steady state.

Finally, we have investigated the properties of the numerical scheme depending on the regularity of the doping concentration: this analysis has shown that the convergence of the numerical scheme is not affected by the abruptness of the doping concentration, at least when the jumps of the doping profile are smeared within a physically reasonable length.

We also mention that the numerical method has been also validated on the solution of the shock-tube problem dealing with the Euler equations of gas dynamics, which, from the mathematical standpoint, corresponds to taking only the hyperbolic part of the hydrodynamic system (1). In this case (results not reported here), the resolution of the discontinuities by the second-order scheme is excellent. Both this fact and the accurate computation of semiconductor shocks produced by the second-order scheme reveal that the discontinuity present at the drain junction of the $n^+ - n - n^+$ diode, due to the strong electric field, is something more challenging to approximate than a shock wave.

Finally, since the experiments show that the amplitude of the spurious oscillations can be reduced by grid refinement, in such a way that a stable and sufficiently accurate solution can be obtained, it seems convenient, also in view of possible 2-D extensions, to combine high resolution schemes with a mesh adaption technique, based on the variation of the electron current profile. This will be the object of a future work.

## Acknowledgements

The authors wish to thank the referees for their helpful comments and suggestions which have considerably improved the quality and impact of the paper.

## References

[1] M.G. Ancona, C.R. DeVore, Numerical simulation of high-field transport using a flux-corrected transport algorithm, in: Proceedings of the Third International Workshop on Computational Electronics, Oregon State University, Portland OR, 1994, p. 256.
[2] M.G. Ancona, Hydrodynamic models of semiconductor electron-transport at high fields, VLSI Des. 3 (1995) 101–114.
[3] A.M. Anile, M. Junk, V. Romano, G. Russo, Cross-validation of numerical schemes for extended hydrodynamical models of semiconductors, Math. Models Methods Appl. Sci. 10 (2000) 833–861.
[4] A.M. Anile, N. Nikiforakis, R.M. Pidatella, Assessment of a high resolution centered scheme for the solution of hydrodynamical semiconductor equations, SIAM J. Sci. Comput. 22 (2000) 1533–1548.
[5] A.M. Anile, V. Romano, G. Russo, Extended hydrodynamical model of carrier transport in semiconductors, SIAM J. Appl. Math. 61 (2000) 74–101.
[6] G. Baccarani, M.R. Wordeman, An investigation of steady-state velocity overshoot effects in Si and GaAs devices, Solid State Electronics 28 (1985) 407–416.
[7] L. Ballestra, S. Micheletti, R. Sacco, F. Saleri, On a viscous-hydrodynamic model for semiconductors: numerical simulation and stability analysis, Comput. Vis. Sci. 4 (2001) 79–86.
[8] L. Ballestra, S. Micheletti, R. Sacco, Semiconductor device simulation using a viscous-hydrodynamic model, Comput. Meth. Appl. Mech. Engrg. 191 (2002) 5427–5446.
[9] L. Ballestra, F. Saleri, Numerical solutions of a viscous-hydrodynamic model for semiconductors: the Supersonic Case, COMPEL: Int. J. Comput. Math. Electr. Electron. Engrg. 22 (2003) 31–54.
[10] K. Bløtekjær, Transport equations for electrons in two-valley semiconductors, IEEE Trans. Electron Dev. ED-17 (1970) 38–47.
[11] D.L. Book, J.P. Boris, Flux-corrected Transport I. SHASTA, a fluid transport algorithm that works, J. Comp. Phys. 11 (1973) 38–69.
[12] D.L. Book, J.P. Boris, K. Hain, Flux-corrected transport II. Generalizations of the method, J. Comp. Phys. 18 (1975) 248–283.
[13] R.S. Chakravarthy, S. Osher, High resolution schemes and the entropy condition, SIAM J. Numer. Anal. 21 (1984) 955–984.
[14] S. Osher, Riemann solvers, the entropy conditions,and difference approximations, SIAM J. Numer. Anal. 21 (1984) 217–234.
[15] E. Fatemi, J. Jerome, S. Osher, Solution of the hydrodynamic model using high-order nonoscillatory shock capturing algorithms, IEEE Trans. Comput.-Aid. Des. 10 (1991) 501–507.
[16] C.L. Gardner, Shock waves in the hydrodynamic model for semiconductor devices, in Semiconductors Part II, in: IMA Volumes in Mathematics and its Applications, vol. 59, Springer, New York, 1994.
[17] C.L. Gardner, J.W. Jerome, D.J. Rose, Numerical methods for the hydrodynamic device model:subsonic flow, IEEE Trans. Comput.-Aid. Des. 8 (1989) 501–507.
[18] A. Harten, High resolution schemes for hyperbolic conservation Laws, J. Comp. Phys. 49 (1983) 357–393.
[19] J.W. Jerome, C.W. Shu, Energy models for one-carrier transport in semiconductor devices, in Semiconductors Part II, in: IMA Volumes in Mathematics and Its Applications, vol. 59, Springer, New York, 1994.
[20] C. Hirsh, in: Numerical Computation of Internal and External Flows, vol. 2, Wiley, Chichester, 1990.
[21] P.L. Roe, Approximate Riemann solvers, parameter vectors, and differences schemes, J. Comp. Phys. 43 (1981) 357–372.
[22] G.D. Van Albada, B. Van Leer, W.W. Roberts, A comparative study of computational methods in cosmic gas dynamics, Astron. Astrophys. 108 (1982) 76–84.